Scientific Research Publishing

American Journal of Climate Change, 2023, 12, 335-358
https://www.scirp.org/journal/ajcc
ISSN Online: 2167-9509
ISSN Print: 2167-9495

Precipitation Cycles Relative to Storm Tracks, ENSO and PDO, and Drought—Continental Interior Central Western USA

Alan L. Mayo

Mayo and Associates LC, Phoenix, AZ, USA
Email: alan_mayo@live.com

How to cite this paper: Mayo, A. L. (2023). Precipitation Cycles Relative to Storm Tracks, ENSO and PDO, and Drought—Continental Interior Central Western USA. *American Journal of Climate Change, 12,* 335-358.
https://doi.org/10.4236/ajcc.2023.123016

Received: May 2, 2023
Accepted: August 15, 2023
Published: August 18, 2023

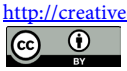

Abstract

Seventy-two years of central western United States precipitation data have been analyzed for storms originating 1000 to 3000 km away from four ocean moisture sources: Arctic, North Pacific, South Pacific, and Gulfs of California and Mexico. Precipitation trends were evaluated relative to precipitation phase, precipitation flux, storm track trajectory, and the sea surface temperature (SST) indices Oceanic Niño Index (ONI), and the Pacific Decadal Oscillation (PDO. The lack of correlation between SST indices with precipitation flux was evaluated. The relationships of meteorological, hydrological and snow droughts were evaluated relative to each other, to the climate change-induced temporal shifts in the timing of mountain snowpack decay, and the timing when North Pacific storm tracks shift from crossing to circumventing the Sierra Nevada Range.

Keywords

Precipitation Cycle, Meteoric Drought, Hydrologic Drought, Snow Drought, Climate Change

1. Introduction

The frequency and intensity of mid-latitude Pacific Ocean cyclonic storms that deliver moisture to the western interior United States have decadal, interannual, and seasonal variability (Chang et al., 2002; Chiodi & Harrison, 2013). This variability has been linked to the El Niño-Southern Oscillation (ENSO), the Pacific Decadal Oscillation (PDO), and other sea surface temperature (SST) and atmospheric conditions (Rohli et al., 2022; Hamamoto & Yasuda, 2021; Seager et al., 2010; Deser et al., 2018). The ENSO index is based on Pacific Ocean SST at

the equator between 120˚ and 170˚ W longitude. The PDO index is a measure of Pacific Ocean SST north of 20˚ north latitude. Western Pacific SSTs contribute to the complex global atmospheric telecommunication (Pan et al., 2017; Alexander et al., 2002), and are used in global climate models (Yeh, 2022; Liu et al., 2022; Capotondi et al., 2020). Predicting the impact of ENSO on weather and climate modeling has been questioned and the strength of using the ENSO index as an indicator in forecast modeling is unclear (Pegion et al., 2022; Evans et al., 2022; Deser et al., 2017; Garfinkel et al., 2013; Capotondi et al., 2015; Takahashi et al., 2018; Garfinkel et al., 2022; Deser at al., 2018; Bayr et al., 2019).

Extratropical Northern Hemisphere atmospheric circulation due to the poleward propagation of Rossby waves promotes ENSO telecommunication across North America (Alexander et al., 2002; Lu et al., 2008; Seager et al., 2010), and ENSO is the most widely used index for predicting interannual and seasonal weather patterns in western North America (Capotondi et al., 2015; Chiodi & Harrison, 2013). ENSO effects are greatest in the Boreal winter (L'Heureux et al., 2015; Jong et al., 2016) when conditions are most favorable for Rosby waves and SST anomalies. During the ENSO warm phase (El Niño) southerly winds carry warmer air northward over the western United States and Canada (NOAA, 2022), while anomalous northerlies bring cooler air to the southeastern United States. The strengthened storm tracks result in above-average precipitation in the southern tier of the United States. La Niña causes the opposite condition with drier conditions in southern California and Arizona, and wetter conditions in the Pacific Northwest (Johnson & Kosaka, 2016). PDO events persist for 20 - 30 years and directly affect the northern Pacific region. Precipitation is typically above average during positive (warm) PDO events and below average during negative (cold) PDO events. Warm PDO episodes bring anomalously warm temperatures to the northwest coast of North America during the winter months (Mantua & Hare, 2002; Wang et al., 2013).

Investigations of ENSO and PDO linkage relative to precipitation and temperature commonly involve modeling experiments (Chen et al., 2020; Sung et al., 2016). At the regional and location specific scale the interannual and seasonal effects of ENSO and PDO on weather patterns are not well understood or predictable (Jong et al., 2016; Maleski & Martinez, 2018; Pavia et al., 2006). The decadal variably of north Pacific storm tracks have been found to be strongly associated with the PDO and linearly independent of ENSO (Gan & Wu, 2013). The natural variability of El Niño on US winter temperatures has in part been attributed to the type of El Niño event—central Pacific (CP) or eastern Pacific (EP), and the ENSO amplitude (Zhang & Wu, 2021; Yu et al., 2012). In southern California PDO has been found to modulate the ENSO-rainfall relationship (Gershunov & Barnett, 1998; Gershunov & Cayan, 2003; Pavia et al., 2016). However, the failed influence of some El Niño events in California has been particularly noteworthy (Lee et al., 2018; Jong et al., 2016). Regional correlation has been found between wet and dry conditions and ENSO and PDO phase linkage.

ENSO and PDO phase linkage has been found to affect drought induced fire occurrences in the Rocky Mountain region (Schoennagel et al., 2005), crop yield in the mid-western United States (Henson et al., 2017), and precipitation in the US Great Plains (Hu & Huang, 2009). ENSO and PDO and their relationships are changing with climate warming particularly when the two are in phase (McPhaden et al., 2020). Cai et al. (2021) found an inter-model consensus of increasing future ENSO rainfall variability with climate change. The temporal structure of the ENSO-PDO relationship is changing, particularly during Boreal winter with more frequent in-phase correlations, and will have more constructive inferences with ENSO-related climates when ENSO and PDO are in phase (Kwon et al., 2013).

The purpose of this investigation is to empirically examine ENSO, PDO, storm tracks, and climate change relative to precipitation cycles in the interior of the western United States.

2. Study Area

The area of investigation is the Great Basin-Rocky Mountain transition zone in the western interior of the United States (**Figure 1**). Both ENSO and PDO may

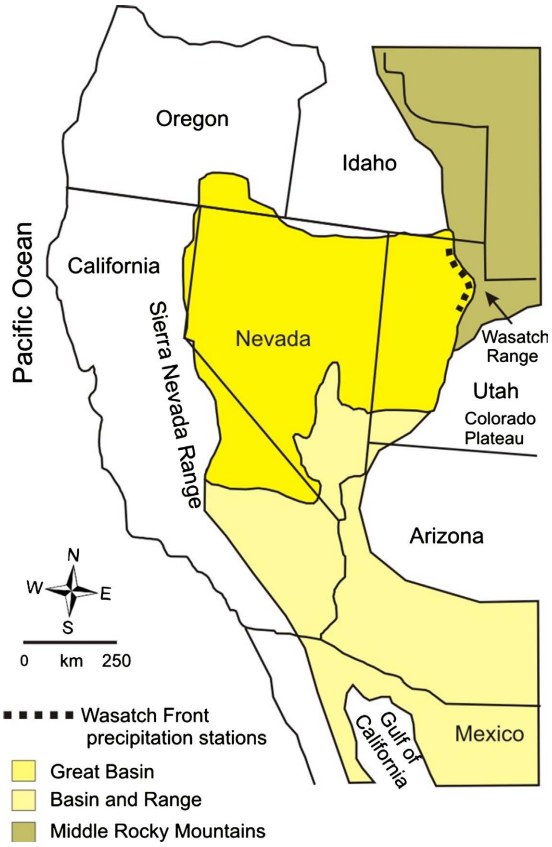

Figure 1. The Great Basin, a vast region of internal drainage in the western United States, occupies the northern portion of the Basin and Range physiographic province. The Wasatch Range is the western edge of the Rocky Mountain physiographic province. Locally the Great Basin portion of this boundary is known as the Wasatch Front.

directly influence storm events, because the precipitation events are driven by storms originating 1000 to 3000 km away in Pacific Ocean between latitudes 70˚ and 15˚ north, and in the Gulfs of California and Mexico between latitudes 30˚ and 15˚ north (Houghton, 1969; Friedman et al., 2002).

The storm sources are: 1) The southern flow of cold polar air originating in the Arctic; 2) The eastern flow of cool North Pacific Ocean air; 3) The northeastern flow of warm South Pacific Ocean air; 4) The northern flow of warm Gulf of California and Gulf of Mexico air (**Figure 2**). What this means is that storms originate from a wide range of SSTs, atmospheric pressures, and air temperatures ranging from the cold Arctic in the north to the warm Pacific and gulfs in the south (Mantua & Hare, 2002; Smith et al., 2015).

Pacific Ocean storms reaching the western interior must navigate a series of orographic features including the near coastal 2100 m high Cascade Range in Washington and Oregon, the 1500 - 2700 m high Sierra Nevada Range in California, and the 2000 - 2700 m high ranges of the Great Basin in Nevada.

3. Methods

Seventy-two years of daily precipitation data (1949-2021) were obtained for 19 permanent weather stations at the Great Basin-Rocky Mountain transition zone

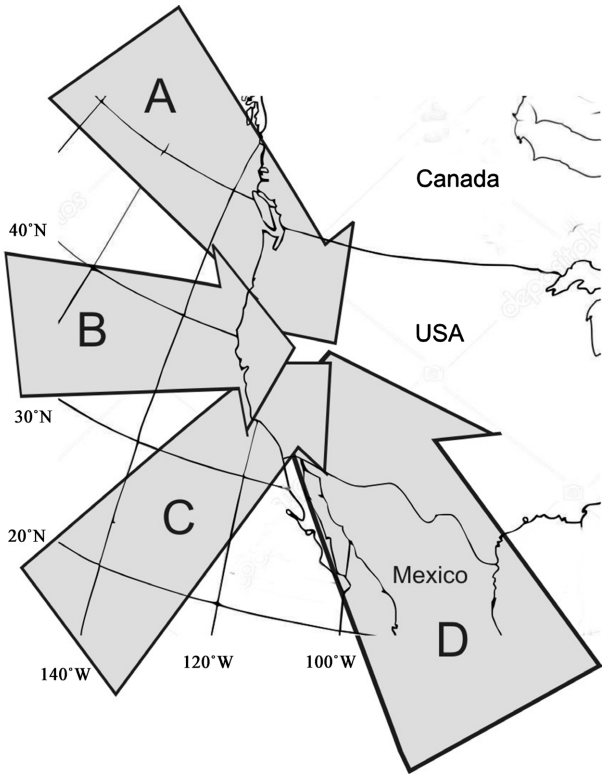

Figure 2. Moisture sources of storms that reach the Wasatch Front in the USA western interior: (A) polar Arctic air; (B) cool North Pacific Ocean air; (C) warm tropical Pacific Ocean air; (D) warm Gulf of California and Gulf of Mexico air. Many Gulf storms are associated with the North American Monsoon (NAM), which provides warm moist air that is responsible for most mid-summer to early fall thunderstorms.

in the western interior of the United States (**Figure 1** (WRCC, 2021)). The stations are located in the Great Basin at the base of the Wasatch Mountain Range in north-central Utah. The daily precipitation amounts were averaged for the 19 stations. The 9251 precipitation days were organized into 3639 storm events. A storm event consists of 1 to 14 days of daily precipitation.

The storm track for the median day of each storm event was determined using the National Oceanic and Atmospheric Administration (NOAA) storm tracking program HYSPLIT (NOAA, 2021a). Storm tracks for air masses 750, 1500 and 3000 m above ground surface (m ags) were calculated for 144-hours prior to reaching the Wasatch Front.

Storm tracks were assigned as originating from the Arctic, North Pacific, South Pacific, and the Gulfs of California and Mexico. Arctic storms originate north of 50˚ north latitude, North Pacific storms originate between 50˚ and 30˚ north latitude, South Pacific originate south of 30˚ north latitude, and gulfs of California and Mexico storms originate in the gulfs south of 30˚ north latitude.

Values for the ONI (NOAA, 2021b) and PDO (NOAA, 2021c) indices were statistically analyzed relative to monthly and seasonal storm tracks, storm events, and precipitation trends using T-test methods at the 95 percent confidence level. The probability of correlation is reported as a p value. A p value < 0.05 means that there is a 95 percent probability that the mean values of the two data sets are the same. Long-term storm phases were identified using a segmented linear regression model (Forkel & Wutzler, 2015).

Local mountain snow pack and river flow data were obtained from SNOTEL (2022), USDA (2022) and USGS (2022). Local mountain air temperature is based on data from the mountain areas Kamas and Silver Lake, Utah. Kamas is located in the intermountain region at 1975 m above mean sea level (m amsl), and Silver Lake is located in the Wasatch Range at 2264 m amsl.

4. Results

4.1. Precipitation Cycles

Precipitation data was organized into water-years (September-August) rather than calendar years to better represent weather cycles. The water year is based on the end of the dry season in August (**Figure 3**). Water-years are designated herein as a single year. For example, the 1949-1950 water-year is designated as 1950. The 25th to 75th percentile ranges of monthly precipitation are 4 or more cm. Months with zero and more that 10 cm have occurred. Calendar year precipitation totals are as much as 46 percent wetter or drier than their corresponding water years and are more than 10 percent wetter or drier half of the time. Water year precipitation ranges from 25.5 to 94.0 cm and averages 49.2 cm. Cumulative 1950-2021 precipitation was 719, 808, 983, and 445 cm for the fall (Sept-Nov), winter (Dec-Feb), spring (Mar-May), and summer months (June-Aug), respectively.

Since 1950 the Wasatch Front has experienced four long-term precipitation phases (**Figure 4**). The first phase (1950-1980) averaged 47.6 cm and had alternating

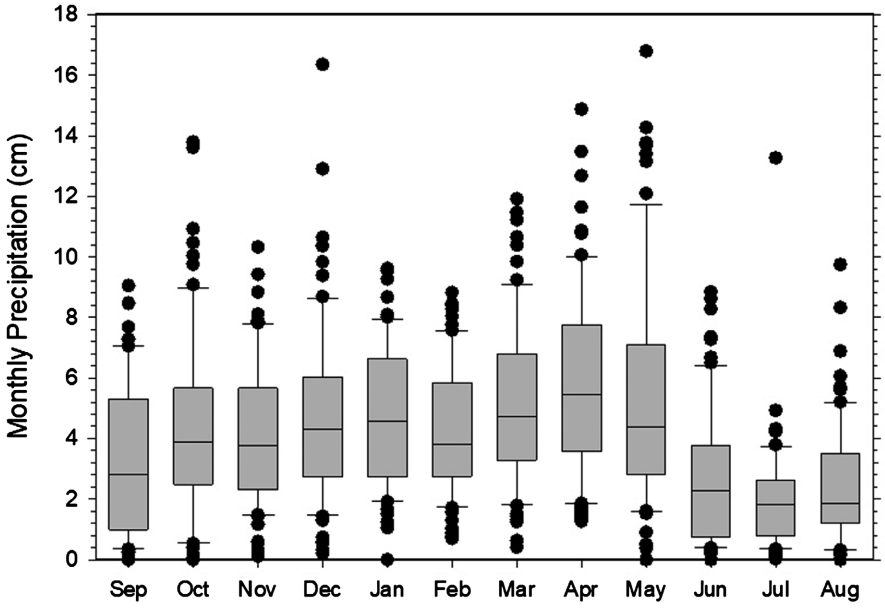

Figure 3. Box plots of Wasatch Front monthly precipitation from September 1949 to August 2021. The months are organized by water year (September-August). The bottom of the box plot is the first quartile (25th percentile) and the top of the plot is the third quartile (75th percentile). The upper and lower whiskers are the maximum and minimum values of the first and third quartiles, respectively. The horizontal line in the box is the median value. The filled circles are outlier data.

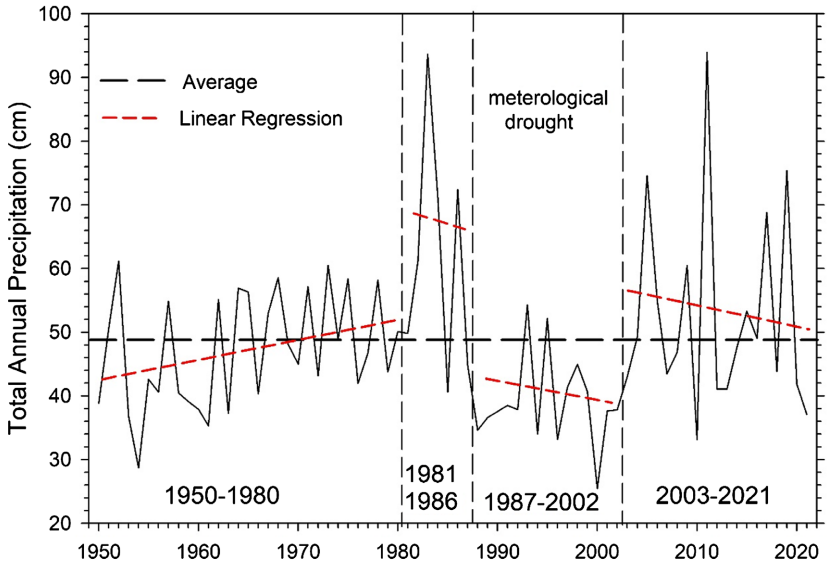

Figure 4. Water year data indicate four precipitation phases since 1950: 1950-1980, 1981-1986, 1987-2002, and 2003-2021. The average water year total precipitation for the period of record is 49.2 cm and is 47.6, 68.7, 39.5, and 52.7 cm for each of the phases, respectively. The trend of precipitation increased during the 1950-1980 phase and declined during each of the subsequent phases. The 1987-2002 phase was a meteorological drought.

wet and dry years. The phase started with a trend of below average precipitation and ended with above average precipitation. This phase was followed by a relatively short and extremely wet (1981-1986) phase that averaged 68.7 cm. The wet

phase was followed by a prolonged meteoric drought (1987-2002) which averaged 39.5 cm. Except for the extremely dry 2010 and 2021 water years (average 35.2 cm) the 2003-2021 phase had above average precipitation (52.7 cm) and most water years had above average precipitation. The general trend of the post 1950-1980 phases was declining precipitation, although there were mid-phase precipitation spikes.

4.2. Storm Tracks

Representative storm tracks for each of the oceanic moisture sources are shown on Figure 5. Arctic storms originate north of 50˚ north and typically reach the

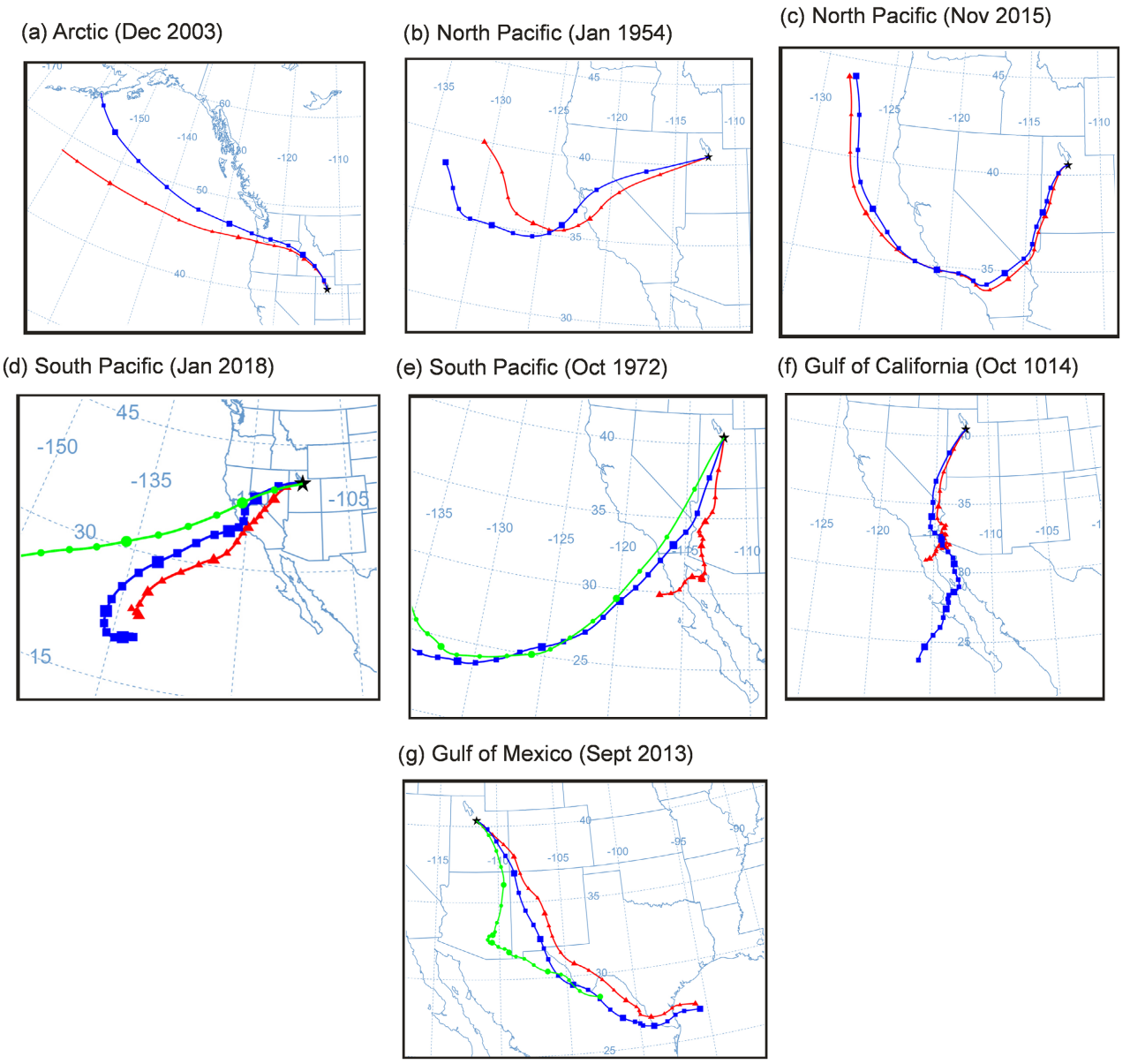

Figure 5. Examples of NOAA HYSPLIT calculated 144-hour storm tracks that reach the Wasatch Front. The symbols on the air mass trajectories are 6-hour intervals. The tracts represent 750 (red), 1500 (blue) and 3000 m (green) above land surface atmospheric conditions. The star is the storm track destination for the HYSPLIT analysis. Storm air masses continued past the star location.

interior of the western US by crossing the Washington and Oregon volcanic mountain ranges (Figure 5(a)). North Pacific storms originate between 50˚ and 30˚ north and typically follow one of two storm tracks. One track crosses the Sierra Nevada Range (Figure 5(b)). The other track flows south along the California coast, circumvents the Sierra Nevada Range, crosses the desert regions of southern California and Nevada, and then flows north along the west side of the Wasatch Range (Figure 5(c)). South Pacific storms originate south of 30˚ north and either cross the southern end of the Sierra Nevada Range (Figure 5(d)) or circumvent the range (Figure 5(e)). Storms circumventing the range travel east across southern California and then skirt the southernmost portion of the Great Basin. Gulfs of California and Mexico storms originate south of 30˚ north (Figure 5(f), Figure 5(g)). These storms first reach the southern end of the Wasatch Range and then are funneled northward along the western side of the range before reaching the Wasatch Front.

5. Analysis

5.1. Precipitation

Arctic and North Pacific storms dominate the fall, winter and spring months (Figure 6(a)). Arctic storms are not a major factor in the summer and North

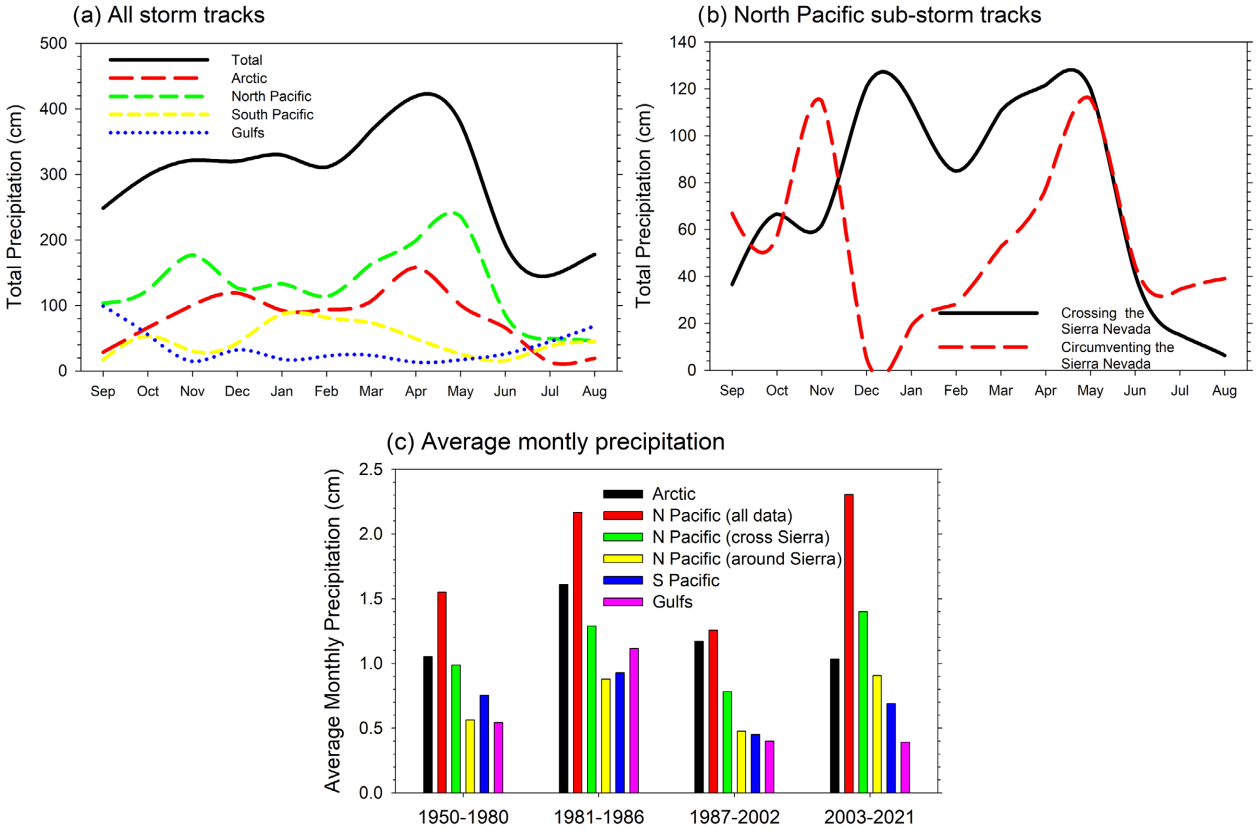

Figure 6. Monthly and precipitation phase precipitation totals for 3639 HYSPLIT storm track trajectories representing 9251 storm-days between 1950 and 2021. The four major trajectories are shown in (a), North Pacific sub-trajectories are in (b), and average water year track monthly averages are in (c).

Pacific storms peak in the winter and early spring. South Pacific storms peak in the winter and early spring. Monsoon storms are significant during the summer months. North Pacific storm tracks are particularly interesting in that about 45 percent of the precipitation comes from storms that circumvent the Sierra Nevada Range. During the winter and early spring most of the North Pacific Storms cross the Range and during the rest of the year many of the storms circumvent the Range (Figure 6(b)). The seasonal pattern of North Pacific storm tracks explains why the Sierra Nevada Range and the high peaks in the Great Basin accumulate significant snow in the winter and, except for late afternoon thunderstorms, are relatively storm free during the summer months.

Between 1950 and 2021 Arctic, North Pacific, South Pacific, and Gulfs of California and Mexico air masses account for 27, 43, 17 and 13 percent, respectively, of the total Wasatch Front precipitation. Although North Pacific storms followed by Arctic storms dominate all precipitation phases (Figure 6(c)), there are significance phase differences. These differences are best understood when the storm track data are parsed by month (Figure 7). During the 1950 -1980 phase Arctic and North Pacific storm precipitation was relatively high in the winter and early spring months and peaked in April and May (Figure 7(a)). The very wet 1981-1986 phase had elevated Arctic and North Pacific precipitation every month except for June, and the Gulfs monsoonal precipitation was unusually great during the summer months (Figure 7(b)). The 1987-2002 meteoric drought years had meager winter and early spring precipitation and quite arid summer months (Figure 7(c)). Arctic storm precipitation was relatively constant from October to May and the precipitation from North Pacific was quite variable. Except for wetter late spring and early summer conditions, the 2003-3021 precipitation phase (Figure 7(d)) was similar to the 1950-1980 phase.

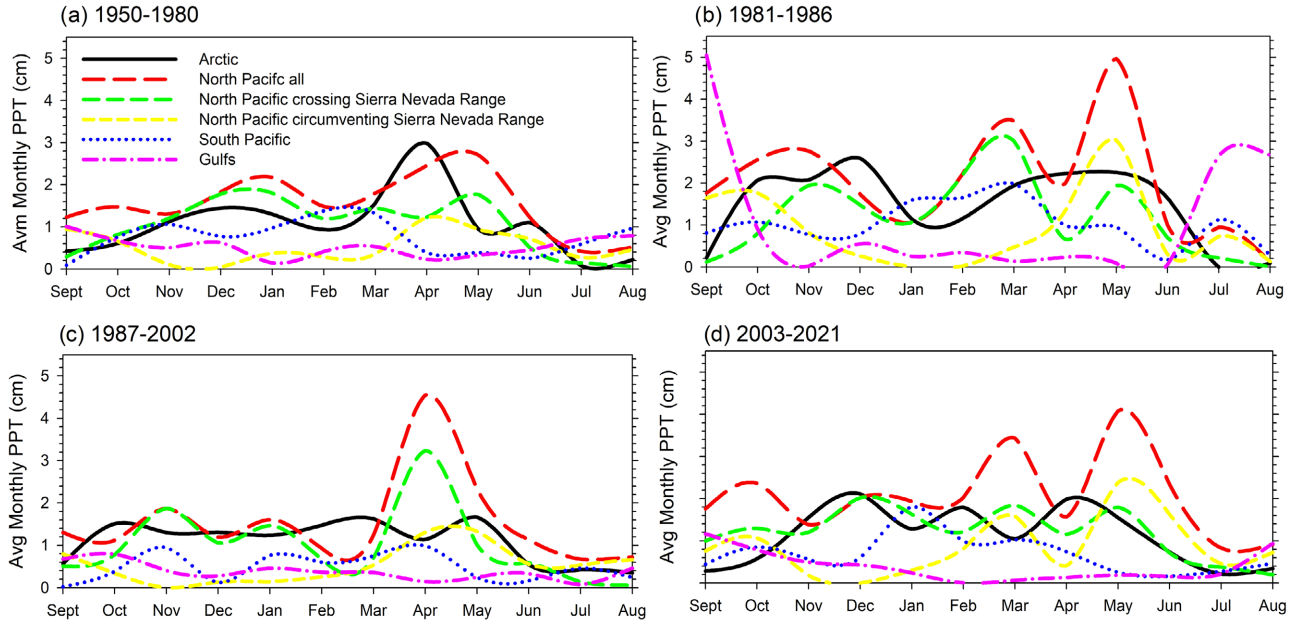

Figure 7. Average Wasatch Front monthly storm track precipitation organized by precipitation phase.

The behavior of North Pacific storms is particularly noteworthy. During the 1950-1980 and the wet 1981-1986 phases most winter and early spring precipitation was from storms that crossed the Sierra Nevada Range. It was not until April that storms circumventing the Sierra Nevada became a major player. During the dry 1987-2002 and the 2003-2021 phases the contributions from storms circumventing the Sierra Nevada Range became significant as early as February.

5.2. Sea Surface Temperature

For the period of record there is no statistical correlation between the total monthly precipitation and the ONI index ($p = 0.75$). Both La Niña and El Niño events each correlate with about 30% of the total precipitation, and during the winter and spring more precipitation fell during La Niña events than during El Niño events (Figure 8(a)). There is a statistical difference between the average monthly precipitation for negative and positive PDO events at the 95 percent confidence level ($p = 0.004$). Negative PDO events correlate with 61% of the total precipitation and positive PDO events only correlate with 39 % of the total precipitation (Figure 8(b)).

The average monthly precipitation during each of the four precipitation phases is plotted relative to the SST indices in Figure 8(c). Average monthly values are used to normalize precipitation because phase durations vary greatly. The figure does not distinguish between storm tracks. The data plot reveals three surprising results. First, although El Niño has historically been considered as a

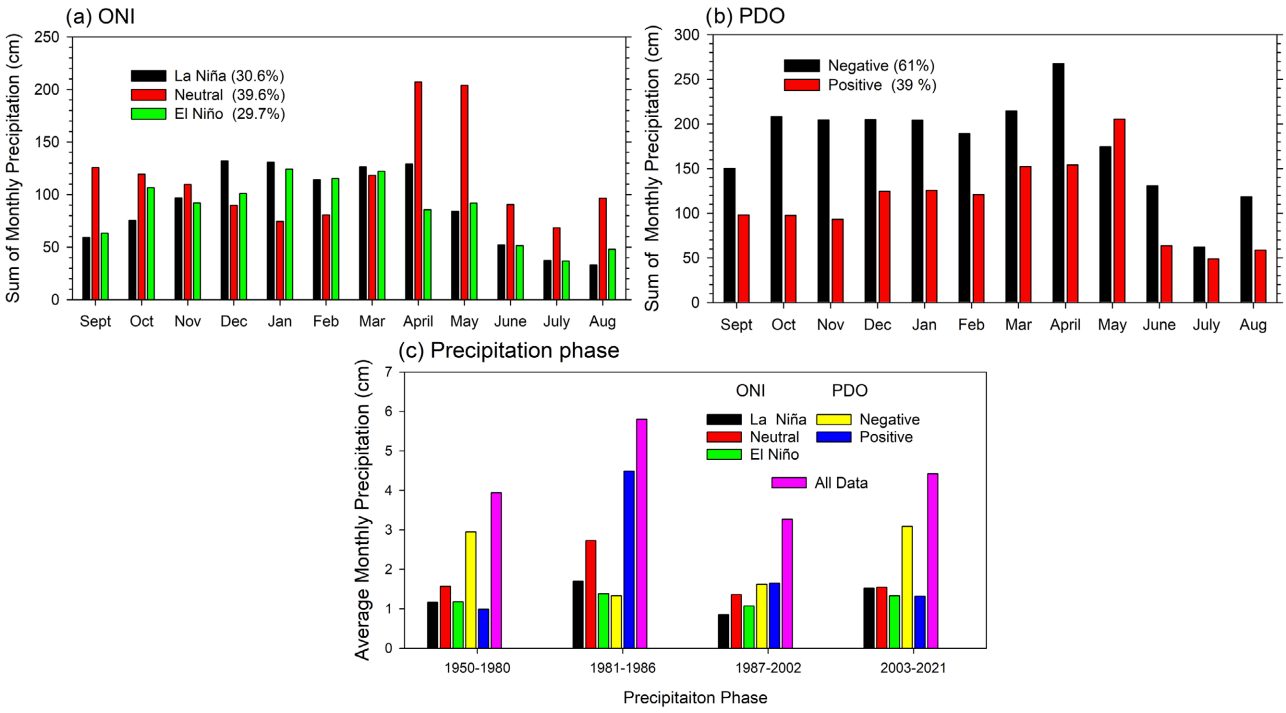

Figure 8. Average monthly precipitation relative to ONI (a) and PDO (b) SST indices, and precipitation phase (c) for all storm tracks combined. Percentages shown in parentheses in (a) and (b) are the percent of the total precipitation for each SST index for the period of record.

predictor for wetter than average winter months in the southwestern United States, El Niño events did not result in wetter conditions for any of the precipitation phases, and there are no statistical differences in average monthly precipitation between El Niño and La Niña events for any of the precipitation phases ($p = 0.22$ to 0.91). Second, the meteorological drought of the 1987-2002 phase and not the hydrological drought of the 2003-2021 phase was the driest period during the past 70 years. A meteorological drought is characterized by low precipitation and a hydrological drought is characterized by reduced river flow and groundwater recharge. The 2003-2021 phase is coincident with what is known as the great southwestern US megadrought (Stahle, 2020). The megadrought is a hydrologic drought. And third, elevated precipitation only correlated with positive PDO during the 1981-1986 wet period.

In an attempt to better understand the relationships between storm tracks, SST, and precipitation phase, Arctic and North Pacific storm tracks have been analyzed relative to the PDO index, and South Pacific and Gulfs storm tracks have been analyzed relative to the ONI index (**Figure 9**). Other storm track-SST configurations do not represent probable atmospheric moisture source-term scenarios. During the more typical precipitation years (1950-1980 and 2002-2021) Arctic and North Pacific events are dominated by negative PDO events, but positive PDO events prevailed during the 1981-1986 wet phase (**Figure 9(a)**). This and the fact that Arctic and North Pacific storms account for most of the precipitation explains why similar precipitation-PDO conditions are found when the storm tracks are considered collectively.

The average monthly South Pacific and Gulfs precipitation was often greater during El Niño than during La Niña (**Figure 9(b)**); however, when the individual months in each phase are analyzed only the Gulfs were statistically different during the 1950-1981 and the 1981-1986 phases (p values 0.002 and 0.003).

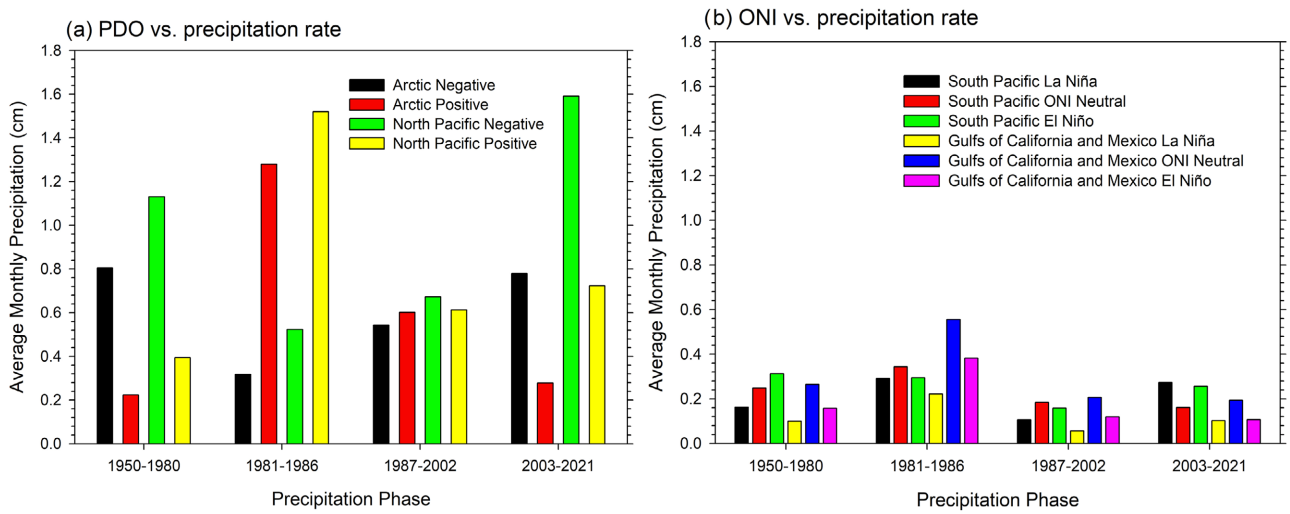

Figure 9. The effects of storm tracks and SST on the average monthly precipitation rates relative to PDO (a) and ONI (b) events for each precipitation phase. Average monthly precipitation is based on the total number of months during each phase. Some months had zero precipitation.

During the 1981-1986 wet phase South Pacific precipitation was similar during El Niño and La Niña, but the Gulf precipitation was unusually great during La Niña. Although the average number of days of precipitation per month mirrors the trends of the average monthly precipitation for each storm track during each precipitation phase, the average precipitation per storm-day varies greatly by storm track and precipitation phase. During the 1950-1980 phase the average storm-day precipitation ranged from 0.3 to 0.45 cm and most storm track/ONI conditions fall in the range of 0.32 to 0.38 cm. The 1981-1986 storm-day precipitation increased greatly during Arctic positive PDO, all North Pacific PDO, and all Gulfs ONI conditions. This increase in storm-days helps explain why the 1981-1986 phase was so wet. Storm-day precipitation for South Pacific storms only increased slightly and decreased for Arctic negative PDO storms. The dry 1987-2002 phase was accompanied by significantly reduced storm-day precipitation for all storm tracks. The number of storm-days in the 2003-2021 phase rebounded after the 1987-2002 phase, but were less than during the 1950-1980 phase.

Except for the 1981-1986 phase, the number of months associated with El Niño and La Niña conditions was similar for each phase. During the 1981-1986 phase there were 11 El Niño months and only three La Niña months. A similar PDO condition occurred during the 1981-1986 phase, when there were only three months of negative PDO and 21 months of positive PDO. During the 1950-1980 and 2002-2021 phases 65 and 70 percent of the months had a negative PDO, respectively. The 1987-2002 phase had almost an identical number of months with positive and negative PDO.

5.3. Precipitation Phase Transition

The transition between precipitation phases is marked by up to 40 cm of an abrupt year-over-year increase or decrease in water year precipitation (**Figure 4**). There is no consistent correlation between ENSO and PDO phases (i.e., El Niño-positive PDO, and La Niña-negative PDO) or with positive or negative ENSO and/or PDO conditions proceeding or during the precipitation phase transitions (**Figure 10**). The 1980-1981 precipitation transition was proceeded with ENSO and PDO in-phase (neutral and near neutral ENSO and slightly positive PDO). ENSO and PDO became out of phase shortly after the transition when PDO became negative. The 1986-1987 precipitation transition occurred during positive and in-phase ENSO and PDO. It is interesting to note that much of the 1987-2002 meteorological drought was accompanied by frequent positive PDO and El Niño conditions. Proceeding of the 2002-2023 precipitation transition there was a strong La Niña and increasing PDO values. Both ENSO and PDO were in-phase during the precipitation transition.

6. Discussion

Precipitation trends, storm tracks, and SST data raises two problematic issues.

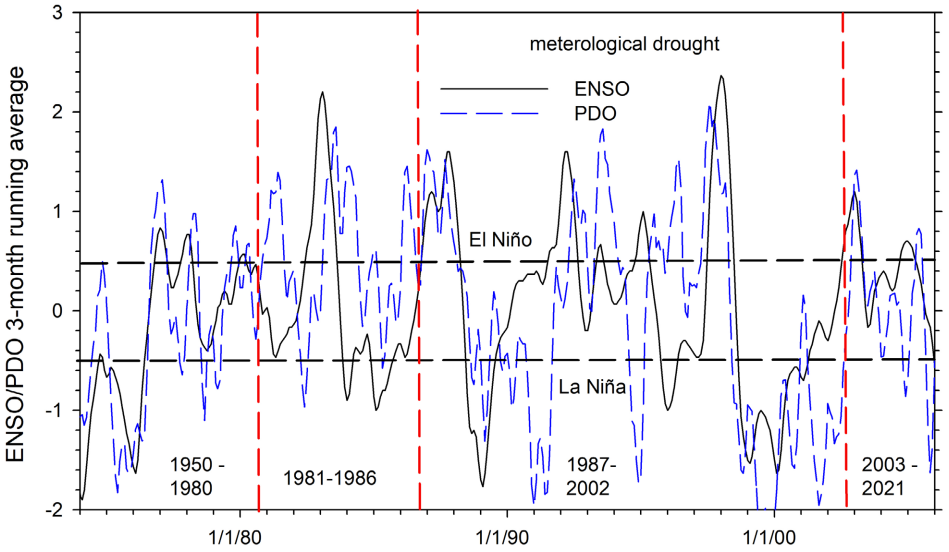

Figure 10. Graph showing 3-month running average ENSO and PDO values during precipitation phase changes. El Niño, neutral, and La Niña conditions are designated with dashed horizontal black lines.

First, wet and dryer precipitation conditions do not statistically correlate with El Niño and La Niña events, and for the period of record months with negative PDO had considerably greater precipitation than months with a positive PDO (**Figure 8(b)**). Several factors may contribute to the general absence of ENSO and precipitation event correlation. Arctic and North Pacific storm tracks and not South Pacific storm tracks are responsible for most of the precipitation (**Figure 9**). This suggests that ENSO does not play a primary role in precipitation totals. The role of positive and negative PDO events is difficult to understand. During the 1950-1980 precipitation phase negative PDO events associated with Arctic and North Pacific storms were significantly more important than during positive PDO events. The fact that negative PDO events correspond with most Arctic and North Pacific total precipitation is more difficult to understand. The northern Great Basin and the Wasatch Front are located at the ENSO forced winter weather transition zone. The transition zone is also known as the ENSO dipole or North American dipole. South of the dipole ENSO is believed to be a major factor in winter weather (Wang et al., 2012; NOAA, 2022). Coupling the ENSO dipole with the PDO and other Pacific Ocean atmospheric and SST oscillations can shift the North American dipole to the north and to the south, thus greatly influencing northern Great Basin and Wasatch Front precipitation rates, precipitation sources, and air temperatures (Brown, 2011; Mantura & Hare, 2002; Smith et al., 2015; Wise, 2010). The net effect of the transitory location of the dipole, due to the interaction of the PDO and ENSO impacted air masses and other atmospheric conditions, is likely the major factor for the lack of correlation between the SST indices, the precipitation phases, and wet and dry episodes.

The second issue is that during most of the 1987-2002 meteorological drought

there was not a corresponding hydrological drought. Except for the 2010 and 2021 water years, the 2003-2021 precipitation phase had above average annual precipitation, but was a hydrological drought have below average river discharge in most years (**Figure 11**). The 2002-2021 phase was coincident with the ongoing western United States megadrought (Heim Jr., 2017; Stahle, 2020). The megadrought, which has severely impacted the states that use river water originating in the Rocky Mountains, the Sierra Nevada Range, and smaller drainage systems in the Great Basin, is epitomized by reduced river flows and low reservoir water levels. For example, Colorado River reservoirs, which are located south of the Wasatch Front and on which 40 million people and ~180,000 km^2 of farmland are dependent, are currently at 30 to 40 percent of capacity and mandatory water rationing has been ordered (NASA, 2022). The Colorado River is the largest drainage network in the Rocky Mountains. Further north, reservoirs that store water associated with Wasatch Front storms were only at 30 to 70 percent of capacity in 2020 and 2021 (Haskell, 2021). It is too early to tell what the effect of the abnormally elevated precipitation during the ongoing 2022-2023 water year will have on the megadrought and if a series of elevated precipitation years will ensue.

Wasatch Front water year precipitation and river runoff from nearby mountain highlands varied greatly during each precipitation phase. During the 1950-1980 phase, when precipitation was about equal to the 70-year average (**Figure 4**) and the average river flow was equal to the 70-year average (**Figure 11**), there were

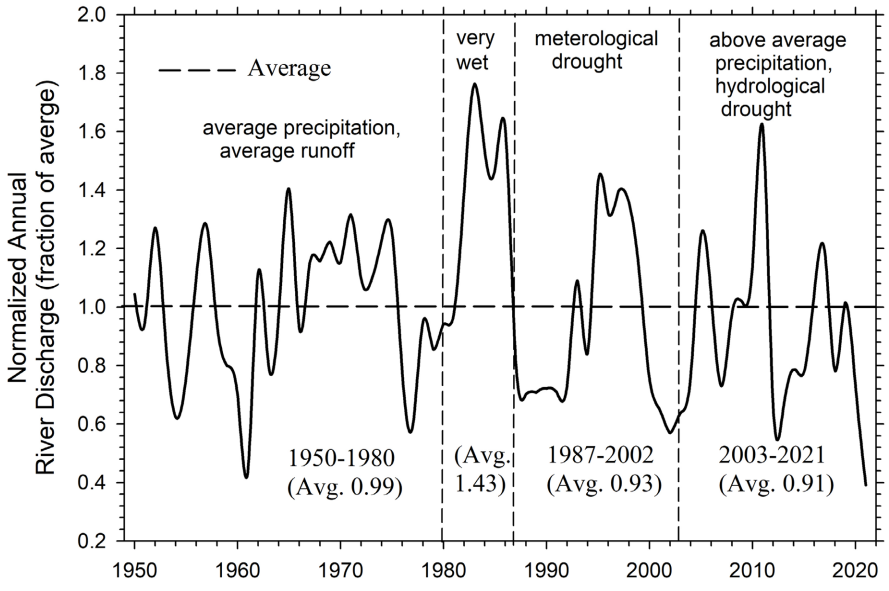

Figure 11. Normalized average water year discharges of non-dammed perennial reach of four rivers that drain into the Great Basin from mountains near the Wasatch Front. The percentage of average discharge during each precipitation phase relative to the 1950-2021 average discharge is shown parentheses. Average discharges range from 89.5 × 10^5 to 56.1 × 10^5 m^3/day. The hydrological drought began in the 2000 water year at the end of the meteorological drought. Much of the 2003-2021 phase was a hydrological draught. Meteorological and hydrological conditions are shown for each phase.

no prolonged periods of below average river discharge. The wet 1981-1986 phase was accompanied by river discharges that were 143 percent of the 70-year average, and the elevated river discharges resulted in severe flooding in the adjacent valleys. The 1987-2002 phase was a meteorological drought with precipitation well below the 70-year average. Average river runoff was only 93 percent of the 70-year average; however, a prolonged hydrological drought did not occur because above average river flow occurred during an extended block of time. During the 2002-2021 phase the average precipitation was greater than the 70-year average, but there was a significant decline in river discharges. This phase can be characterized as a hydrological drought with average river discharge of only 91 percentage of the 70-year average, and most water years had below average discharge. The hydrologic drought was compounded during the 2020-2021 water years when a meteorological drought also occurred.

The relationships between the meteorological and the hydrological droughts are not straightforward. In the American southwest river flows are highly dependent on the melting of the mountainous snowpack (USGS, 2023). There is a striking difference in the snow pack water content between water years with less than 90 percent and years with more than 110 percent of the average annual precipitation (**Figure 12(a)**). During wet years the peak average water content is about 62 cm in mid-March compared to 40 cm in early march during dryer years. It is not until early May that the water content of wet year snow pack declines to 40 cm. The apparent paradox of the Wasatch Front's above average annual precipitation during the 2002-2021 megadrought correlates with the change in the timing of mountain snowpack melting, and the change in the seasonal trend of North Pacific storm tracks. Except for the very wet 1981-1986 phase, the average snowpack water content of all precipitation phases was similar during the fall and winter months (**Figure 12(c)**). Elevated snow pack accumulation began early in 1981-1986 phase and continued well into April. During the 1950-1980 phase average snowpack peaked in April and lingered well into May. Since then, the average snowpack water content peaked in March and declined rapidly after that. Snow water equivalent deficits have been described as snow droughts (Harpold et al., 2017; Huning & Aghakouchak, 2020; Gottlieb & Mankin, 2021).

The early decay of the snowpack has a significant impact on river discharge. From late August to April the rivers are supported by groundwater base flow (**Figure 13**). The flow increases rapidly in response to the spring snow melt starting in April and peaking in May to June. The change in the peak of the snow pack water content from May during the 1950-1980 phase to March and April since the end of the 1981-1986 phase means that less snowmelt water has been available for runoff. The overall reduction in average river discharge (**Figure 12(b)**) is attributed to this shift in the snow pack water content. The early loss of snowpack corresponds with increasing springtime air temperatures in the mountainous region (**Figure 14**). The increase is most significant in March and

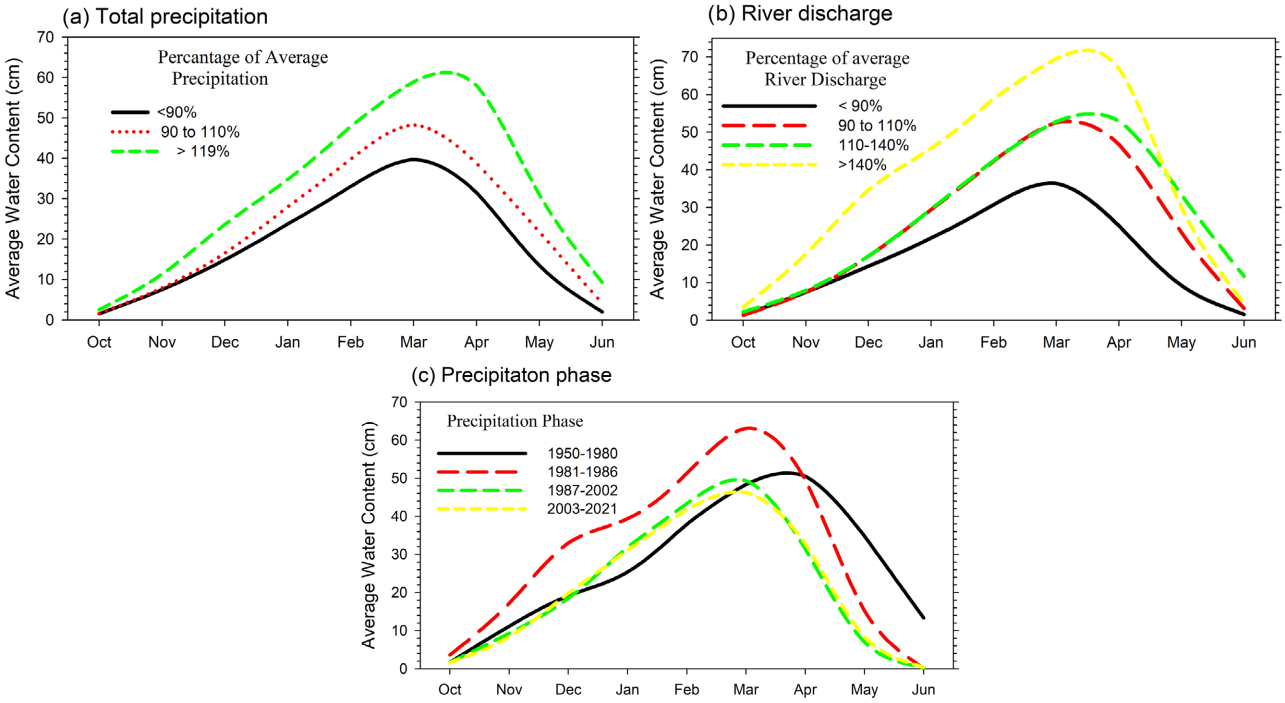

Figure 12. Temporal changes in average water content equivalent of Wasatch Range and adjacent mountain highlands snowpacks during each of the four precipitation phases (a), as a percentage of total average precipitation (b) and, as a percentage of average river discharge (c).

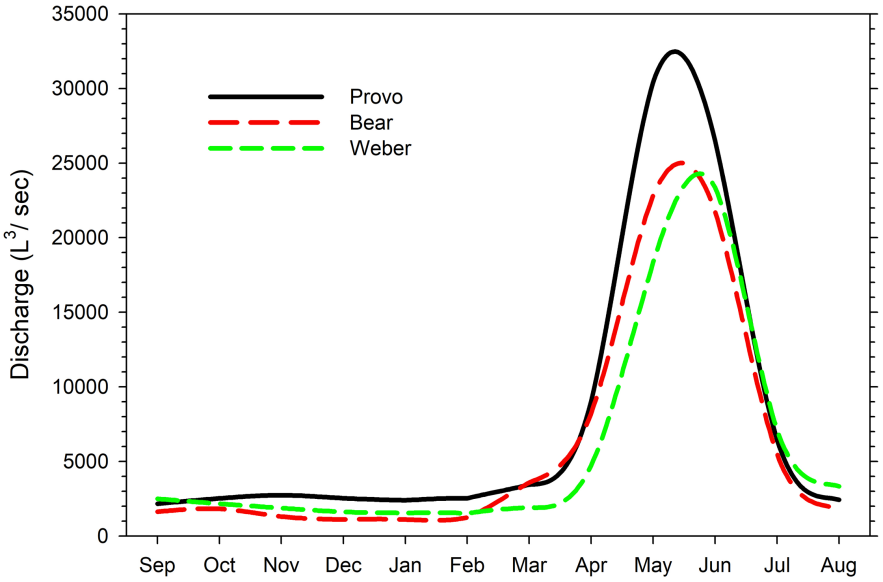

Figure 13. Average of the 70-year monthly discharge rates of free-flowing reaches of three major rivers that are supported by storms that cross the Wasatch Front.

April. In the winter when the air temperature is cold there is an overall increase in the snow pack and snow loss is the result of sublimation rather than snowmelt. The progressive increase in the early warming of March and April air temperatures means that less of the late spring precipitation fell as snow, and the snowmelt period began sooner and was lengthened. Lengthening the snowmelt

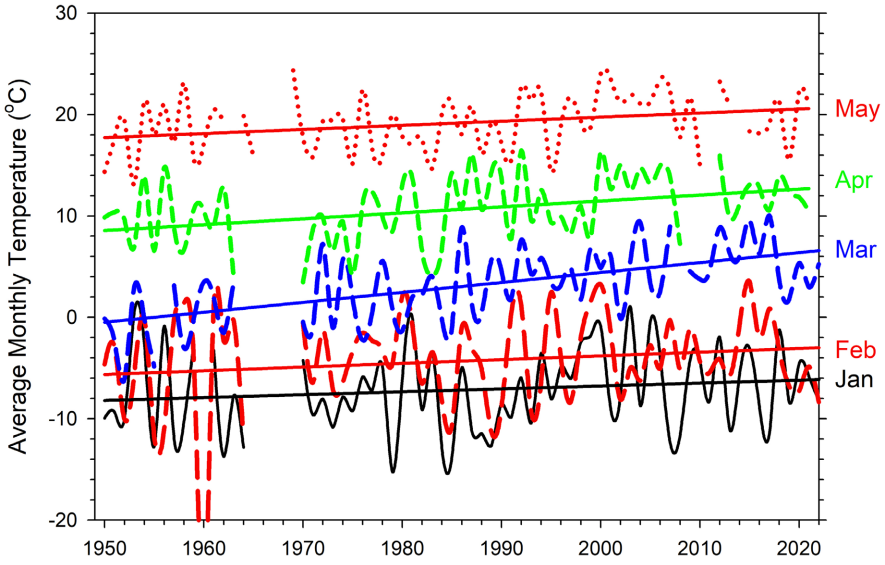

Figure 14. The trend of increasing average winter and springtime air temperature at Kamas Utah. Kamas is located in the in the Wasatch Range at an elevation of 1,975 m amsl. The solid sloping lines are regression analysis trends at the 95 percent confidence level.

period reduces volume of the water available for the May and June snowmelt runoff surge that is necessary for peaking river discharges. Much of the early snowmelt was likely lost to evaporation and soil moisture replenishment rather than as part of the May-June snowmelt surge.

The post 1986 reduction in average river discharge also corresponds with the change in behavior of the North Pacific storms when the fraction of storms circumventing the Sierra Nevada Range increased (**Figure 6(b)**). During the 1950-1980 and the wet 1981-1986 phases most winter and early spring precipitation was from storms that crossed the Sierra Nevada Range. It was not until April that the number of storms circumventing the Sierra Nevada Range became important. During the dry 1987-2002 and the more typical 2003-2021 phase the contributions from storms circumventing the Sierra Nevada Range became significant as early as April and February, respectively (**Figure 7(b)**, **Figure 7(c)**). This one to two-month shift likely had a profound effect on the fate of precipitation, particularly the accumulation of snow in the mountains. Storms that cross the Sierra Nevada must travel from air masses that maintain cold conditions as the storms cross the higher elevation ranges of the Sierra Nevada and the Great Basin. The air temperature of storms that circumvent the Sierra Nevada Range becomes progressively warmer as the storms travel south along the coast. For example, the average February-March minimum and maximum air temperatures at Lake Tahoe, California are −5.6˚C and 8.3˚C respectively, and the average temperatures in San Diego, California are 11.7˚C and 18.8˚C respectively. Lake Tahoe has a winter snow pack is at an elevation of 2144 m amsl in the Sierra Nevada Range, and San Diego is at sea level south of the Sierra Nevada Range near the USA-Mexico border. Precipitation from colder air crossing the Sierra Nevada Range and the Great Basin is more likely to result in snow accumulation

in the Wasatch Range than the warmer air that circumvents the range.

The cause of the early springtime mountain air temperature warming, and the springtime change in North Pacific storm tracks is attributed to climate change. Near the Wasatch Front there has been a consistent trend of increasing springtime mountain air temperature and since about 2000 there is has been significant increase in the Arctic and North Pacific Ocean air temperatures (Scott, 2022). Arctic and North Pacific air temperatures greatly influence storm patterns of the North Pacific storms in the south (Song et al, 2021; Johnstone & Mantua, 2014), and the trend of the accelerated loss of Arctic Sea ice in the north (Connolly et al., 2017; Fetterer et al., 2022; NSIDC, 2022).

7. Conclusion

Precipitation cycles are best understood when organized by water year rather than calendar year. The water year in the study area is September to August. Between 1950 and 2021 four meteorological precipitation phases occurred: 1) 1950-1980 with average annual precipitation; 2) an extremely wet 1981-1986; 3) a meteorological drought during 1987-2002; 4) slightly above average precipitation in 2003-2021. 2010 and 2021 suffered a meteorological drought.

Storms originate from ocean sources 1000 to 3000 km away, and travel along four storm tracks: Arctic, North Pacific, South Pacific, and the Gulfs of California and Mexico. These air masses account for 27, 43, 17 and 13 percent of the total precipitation, respectively. The behavior of North Pacific storms is particularly noteworthy. Prior to 1987 most winter and early spring storms crossed the Sierra Nevada Range. After 2002 the contributions from storms circumventing the Sierra Nevada Range became significant as early as February.

Although SSTs are influenced by global atmosphere temperate increases, wet and dry water years do not correspond to El Niño and La Niña events, or consistently with positive and negative PDO phases. The transitions between meteorological phases do not consistently correspond with ENSO and PDO positive or negative conditions or with ENSO and PDO in-phase conditions. During the very wet 1981-1986 phase, the PDO was mostly positive, but unexpectedly mostly negative during other precipitation phases. The lack of correlation between the ONI and PDO indices may be influenced by 1) the limited amount of precipitation from South Pacific and Gulf storms and 2) the north-south migration of the ENSO Dipole (aka North American Dipole). The Dipole migration is attributed to the interaction of the PDO and ENSO impacted air masses, and other atmospheric conditions.

The Wasatch Front's meteorological and hydrological droughts are out of sync. During most of the 1987-2002 meteorological drought, there was not a corresponding hydrological drought, and during the 2002-2021 phase, there was above average annual precipitation while the western US experienced the megadrought. The absence of a hydrological drought during much of the 1987-2002 precipitation phase is likely due to two conditions. The meteorological drought

followed an extremely wet period when soil conditions were fully saturated, and the trend of early springtime mountain air temperature increases had not reached a critical level to induce the early loss of mountain snowpack. The 2000-2021 hydrologic drought is attributed to a snow drought that is due to a combination of factors. First, the progressive temporal increases in the warming of March and April mountain air temperatures caused: 1) some of the late spring precipitation to fall as rain rather than as snow; 2) the snowmelt period to begin sooner and lengthen. Early and longer snowmelt episodes reduce the volume of water available for the May and June snowmelt runoff surge that is necessary for peaking river discharges. And second, the shift in the timing when North Pacific storms began to circumvent the Sierra Nevada Range from April to February likely had a profound effect on the fate of precipitation, particularly the accumulation of late season snow in the mountains. Storms circumventing the Range tend to yield rain rather than snow because the air masses warm as they circumvented the Sierra Nevada Range. The shift in the timing of mountain air temperature warming and the springtime change in North Pacific storm tracks has occurred when global atmospheric temperatures have increased and are likely influenced by climate change. This idea is consistent with analysis of the climate induced decline in river flows worldwide (Gudmundsson et al., 2021).

In summary, based on an analysis of 72 years of precipitation data El Niño and La Niña and other sea surface temperature indices do not correlate with overall wet or dry winter conditions and the indexes are not predictors of upcoming above or below average precipitation at the Great Basin-Rocky Mountain transition zone in the continental interior western United States. The so called 20-year mega-drought occurred during a time of above average precipitation, and the drought correlates with a shortage of spring-time mountain snow due to climate change induced spring time air temperature warming and the shift in the pattern of North Pacific Ocean storm tracks.

Conflicts of Interest

The author declares no conflicts of interest regarding the publication of this paper.

References

Alexander, M. A., Bladé, I., Newman, M., Lanzante, J. R., Lau, N.-C., & Scott, J. D. (2002). The Atmospheric Bridge: The Influence of ENSO Teleconnections on Air-Sea Interaction over the Global Oceans. *Journal of Climate, 15,* 2205-2231. https://doi.org/10.1175/1520-0442(2002)015<2205:TABTIO>2.0.CO;2

Bayr, T., Domeisen, D. I., & Wengel, C. (2019). The Effect of the Equatorial Pacific Cold SST Bias on Simulated ENSO Teleconnections to the North Pacific and California. *Climate Dynamics, 53,* 3771-3789. https://doi.org/10.1007/s00382-019-04746-9

Brown, D. P. (2011). Winter Circulation Anomalies in the Western United States Associated with Antecedent and Decadal ENSO Variability. *Earth Interactions, 15,* 1-12. https://doi.org/10.1175/2010EI334.1

Cai, W., Santoso, A., Collins, M. et al. (2021). Changing El Niño-Southern Oscillation in a Warming Climate. *Nature Reviews Earth & Environment, 2,* 628-644. https://doi.org/10.1038/s43017-021-00199-z

Capotondi, A., Deser, C., Phillips, A. S., Okumura, Y., & Larson, S. M. (2020). ENSO and Pacific Decadal Variability in the Community Earth System Model Version 2. *Journal of Advances in Modeling Earth Systems, 12,* e2019MS002022. https://doi.org/10.1029/2019MS002022

Capotondi, A., Wittenberg, A. T., Newman, M., Di Lorenzo, E., Yu, J. Y., Braconnot, P., Cole, J., Dewitte, B., Giese, B., Guilyardi, E., Jin, F.-F., Karnauskas, K., Kirtman, B., Lee, T., Schneider, N., Xue, Y., & Yeh, S.-W. (2015). Understanding ENSO Diversity. *Bulletin of the American Meteorological Society, 96,* 921-938. https://doi.org/10.1175/BAMS-D-13-00117.1

Chang, E. K. M., Lee, S., & Swanson, K. L. (2002). Storm Track Dynamics. *Journal of Climate, 15,* 2163-2183. https://doi.org/10.1175/1520-0442(2002)015<02163:STD>2.0.CO;2

Chen, R., Simpson, I. R., Deser, C., & Wang, B. (2020). Model Biases in the Simulation of the Springtime North Pacific ENSO Teleconnection. *Journal of Climate, 33,* 9985-10002. https://doi.org/10.1175/JCLI-D-19-1004.1

Chiodi, A. M., & Harrison, D. E. (2013). El Niño Impacts on Seasonal U.S. Atmospheric Circulation, Temperature, and Precipitation Anomalies: The OLR-Event Perspective. *Journal of Climate, 26,* 822-837. https://doi.org/10.1175/JCLI-D-12-00097.1

Connolly, R., Connolly, M., & Soon, W. (2017). Re-Calibration of Arctic Sea Ice Extent Datasets Using Arctic Surface Air Temperature Records. *Hydrological Sciences Journal, 62,* 1317-1340. https://doi.org/10.1080/02626667.2017.1324974

Deser, C., Simpson, I. R., McKinnon, K. A., & Phillips, A. S. (2017). The Northern Hemisphere Extratropical Atmospheric Circulation Response to ENSO: How Well Do We Know It and How Do We Evaluate Models Accordingly? *Journal of Climate, 30,* 5059-5082. https://doi.org/10.1175/JCLI-D-16-0844.1

Deser, C., Simpson, I. R., Phillips, A. S., & McKinnon, K. A. (2018). How Well Do We Know ENSO's Climate Impacts over North America, and How Do We Evaluate Models Accordingly? *Journal of Climate, 31,* 4991-5014. https://doi.org/10.1175/JCLI-D-17-0783.1

Evans, C. P., Coats, S., Carrillo, C. M., Li, X., Alessi, M. J., Herrera, D. A., Benton, B.N., & Ault, T. R. (2022). Intrinsic Century-Scale Variability in Tropical Pacific Sea Surface Temperatures and their Influence on Western US Hydroclimate. *Geophysical Research Letters, 49,* e2022GL099770. https://doi.org/10.1029/2022GL099770

Fetterer, F., Knowles, K., Meier, W., Savoie, M., & Windnagel, A. K. (2002). *Sea Ice Index.* NSIDC: National Snow and Ice Data Center.

Forkel, M., & Wutzler, T. (2015). *Greenbrown—Land Surface Phenology and Trend Analysis.* A Package for the R Software. Version 2.2, 2015-04-15. R-Forge. http://greenbrown.r-forge.r-project.org/

Friedman, I., Harris, J. M., Smith, G. I., & Johnson, C. A. (2002). Stable Isotope Composition of Waters in the Great Basin, United States 1. Air-Mass Trajectories. *Journal of Geophysical Research: Atmospheres, 107,* ACL 14-1-ACL 14-14. https://doi.org/10.1029/2001JD000565

Gan, B., & Wu, L. (2013). Seasonal and Long-Term Coupling between Wintertime Storm Tracks and Sea Surface Temperature in the North Pacific. *Journal of Climate, 26,* 6123-6136. https://doi.org/10.1175/JCLI-D-12-00724.1

Garfinkel, C. I., Chen, W., Li, Y., Schwartz, C., Yadav, P., & Domeisen, D. (2022). The Winter North Pacific Teleconnection in Response to ENSO and the MJO in Operational Subseasonal Forecasting Models Is Too Weak. *Journal of Climate, 35,* 4413-4430. https://doi.org/10.1175/JCLI-D-22-0179.1

Garfinkel, C. I., Hurwitz, M. M., Waugh, D. W., & Butler, A. H. (2013). Are the Teleconnections of Central Pacific and Eastern Pacific El Niño Distinct in Boreal Wintertime? *Climate Dynamics, 41,* 1835-1852. https://doi.org/10.1007/s00382-012-1570-2

Gershunov, A., & Barnett, T. P. (1998). Interdecadal Modulation of ENSO Teleconnections. *Bulletin of the American Meteorological Society, 79,* 2715-2726. https://doi.org/10.1175/1520-0477(1998)079<2715:IMOET>2.0.CO;2

Gershunov, A., & Cayan, D. R. (2003). Heavy Daily Precipitation Frequency over the Contiguous United States: Sources of Climatic Variability and Seasonal Predictability. *Journal of Climate, 16,* 2752-2765. https://doi.org/10.1175/1520-0442(2003)016<2752:HDPFOT>2.0.CO;2

Gottlieb, A. R., & Mankin, J. S. (2021). Observing, Measuring, and Assessing the Consequences of Snow Drought. *Bulletin of the American Meteorological Society, 103,* E1041-E1060. https://doi.org/10.1175/BAMS-D-20-0243.1

Gudmundsson, L., Boulange, J., Do, H. X., Gosling, S. N., Grillakis, M. G., Koutroulis, A. G., Leonard, M., Liu, J., Müller Schmied, H., Papadimitriou, L., Pokhrel, Y., Seneviratne, S. I., Satoh, Y., Thiery, W., Westra, S., Zhang, X., & Zhao, F.(2021). Globally Observed Trends in Mean and Extreme River Flow Attributed to Climate Change. *Science, 71,* 1159-1162. https://doi.org/10.1126/science.aba3996

Hamamoto, M., & Yasuda, I. (2021). Synchronized Interdecadal Variations behind Regime Shifts in the Pacific Decadal Oscillation. *Journal of Oceanography, 77,* 383-392. https://doi.org/10.1007/s10872-021-00592-8

Harpold, A. A., Dettinger, M., & Rajagopal, S. (2017). Defining Snow Drought and Why It Matters. *EOS, 98.* https://doi.org/10.1029/2017EO068775

Haskell, L. (2021). *Reservoir Storage Level Drought Statistics.* Utah Division of Water Resources.

Heim Jr., R. R. (2017). A Comparison of the Early Twenty-First Century Drought in the United States to the 1930s and 1950s Drought Episodes. *Bulletin of the American Meteorological Society, 98,* 2579-2592. https://doi.org/10.1175/BAMS-D-16-0080.1

Henson, C., Market, P., Lupo, A., & Guinan, P. (2017). ENSO and PDO-Related Climate Variability Impacts on Midwestern United States Crop Yields. *International Journal of Biometeorology, 61,* 857-867. https://doi.org/10.1007/s00484-016-1263-3

Houghton, J. G. (1969). *Characteristics of Rainfall in the Great Basin.* Desert Research Institute, University of Nevada System.

Hu, Z.-Z., & Huang, B. (2009). Interferential Impact of ENSO and PDO on Dry and Wet Conditions in the U.S. Great Plains. *Journal of Climate, 22,* 6047-6065. https://doi.org/10.1175/2009JCLI2798.1

Huning, L. S., & AghaKouchak, A. (2020). Global Snow Drought Hot Spots and Characteristics. *Proceedings of the National Academy of Sciences of the United States of America, 117,* 19753-19759. https://doi.org/10.1073/pnas.1915921117

Johnson, N. C., & Kosaka, Y. (2016). The Impact of Eastern Equatorial Pacific Convection on the Diversity of Boreal Winter El Niño Teleconnection Patterns. *Climate Dynamics, 47,* 3737-3765. https://doi.org/10.1007/s00382-016-3039-1

Johnstone, J. A., & Mantua, N. J. (2014). Atmospheric Controls on Northeast Pacific Temperature Variability and Change, 1900-2012. *Proceedings of the National Academy of Sciences of the United States of America, 111,* 14360-14365. https://doi.org/10.1073/pnas.1318371111

Jong, B. T., Ting, M., & Seager, R. (2016). El Niño's Impact on California Precipitation: Seasonality, Regionality, and El Niño Intensity. *Environmental Research Letters, 11,* Article ID: 054021. https://doi.org/10.1088/1748-9326/11/5/054021

Kwon, M., Yeh, S.-W., Park, Y.-G., & Lee, Y.-K. (2013). Changes in the Linear Relationship of ENSO-PDO under the Global Warming. *International Journal of Climatology, 33,* 1121-1128. https://doi.org/10.1002/joc.3497

L'Heureux, M. L., Tippett, M. K., & Barnston, A. G. (2015). Characterizing ENSO Coupled Variability and Its Impact on North American Seasonal Precipitation and Temperature. *Journal of Climate, 28,* 4231-4245. https://doi.org/10.1175/JCLI-D-14-00508.1

Lee, S.-K., Lopez, H., Chung, E.-S., DiNezio, P., Yeh, S.-W., & Wittenberg, A. T. (2018). On the Fragile Relationship between El Niño and California Rainfall. *Geophysical Research Letters, 45,* 907-915. https://doi.org/10.1002/2017GL076197

Liu, B., Gan, B., Cai, W., Wu, L., Geng, T., Wang, H., Wang, S., Jing, Z., & Jia, F. (2022). Will Increasing Climate Model Resolution Be Beneficial for ENSO Simulation? *Geophysical Research Letters, 49,* e2021GL096932. https://doi.org/10.1029/2021GL096932

Lu, J., Chen, G., & Frierson, D. M. (2008). Response of the Zonal Mean Atmospheric Circulation to El Niño versus Global Warming. *Journal of Climate, 21,* 5835-5851. https://doi.org/10.1175/2008JCLI2200.1

Maleski, J. J., & Martinez, C. J. (2018). Coupled Impacts of ENSO AMO and PDO on Temperature and Precipitation in the Alabama-Coosa-Tallapoosa and Apalachicola-Chattahoochee-Flint River Basins. *International Journal of Climatology, 38,* e717-e728. https://doi.org/10.1002/joc.5401

Mantua, N. J., & Hare, S. R. (2002). The Pacific Decadal Oscillation. *Journal of Oceanography, 58,* 35-44. https://doi.org/10.1023/A:1015820616384

Mantura, N. J., & Hare, S. R., (2002). The Pacific-Decadal Oscillation. *Journal of Ocean, 58,* 35-55.

McPhaden, M. J., Santoso, A., & Cai, W. (2020). El Niño Southern Oscillation in a Changing Climate. In *Geophysical Monograph Series* (Vol. 253). John Wiley & Sons. https://doi.org/10.1002/9781119548164

NASA (2022). *Lake Mead Drops to a Record Low.* Earth Observatory.

NOAA (2021a). https://www.ready.noaa.gov/HYSPLIT.php

NOAA (2021b). *Cold & Warm Episodes by Season.* https://origin.cpc.ncep.noaa.gov/products/analysis_monitoring/ensostuff/ONI_v5.php

NOAA (2021c). *Pacific Decadal Oscillation (PDO).* https://www.psl.noaa.gov/pdo/

NOAA (2022). *What Are El Niño and La Niña.* https://oceanservice.noaa.gov/facts/ninonina.html

NSIDC (2022). *Sea Ice Index.* National Snow and Ice Data Center.

Pan, Z., Shi, C., Kumar, S., & Gao, Z. (2017). North Pacific SST Forcing on the Central United States "Warming Hole" as Simulated in CMIP5 Coupled Historical and Uncoupled AMIP Experiments. *Atmosphere-Ocean, 55,* 57-77. https://doi.org/10.1080/07055900.2016.1261690

Pavia, E. G., Graef, F., & Fuentes-Franco, R. (2016). Recent ENSO-PDO Precipitation Relationships in the Mediterranean California Border Region. *Atmospheric Science Letters, 17,* 280-285. https://doi.org/10.1002/asl.656

Pavia, E. G., Graef, F., & Reyes, J. (2006). PDO-ENSO Effects in the Climate of Mexico. *Journal of Climate, 19,* 6433-6438. https://doi.org/10.1175/JCLI4045.1

Pegion, K., Becker, E. J., & Kirtman, B. P. (2022). Understanding Predictability of Daily

Southeast US Precipitation Using Explainable Machine Learning. *Artificial Intelligence for the Earth Systems, 1,* e220011. https://doi.org/10.1175/AIES-D-22-0011.1

Rohli, R. V., Snedden, G. A., Martin, E. R., & DeLong, K. L. (2022). Impacts of Ocean-Atmosphere Teleconnection Patterns on the South-Central United States. *Frontiers in Earth Science, 10,* Article 934654. https://doi.org/10.3389/feart.2022.934654

Schoennagel, T., Veblen, T. T., Romme, W. H., Sibold, J. S., & Cook, E. R. (2005). ENSO and PDO Variability Affect Drought-Induced Fire Occurrence in Rocky Mountain Subalpine Forests. *Ecological Applications, 15,* 2000-2014. https://doi.org/10.1890/04-1579

Scott, M. (2022). *2020 Arctic Air Temperatures Continue a Long-Term Warming Streak.* NOAA.

Seager, R., Naik, N., Ting, M., Cane, M.A., Harnik, N., & Kushnir, Y. (2010). Adjustment of the Atmospheric Circulation to Tropical Pacific SST Anomalies: Variability of Transient Eddy Propagation in the Pacific-North America Sector. *Quarterly Journal of the Royal Meteorological Society, 136,* 277-296. https://doi.org/10.1002/qj.588

Smith, K., Strong, C., & Wang, S. Y. (2015). Connectivity between Historical Great Basin Precipitation and Pacific Ocean Variability: A CMIP5 Model Evaluation. *Journal of Climate, 28,* 6096-6112. https://doi.org/10.1175/JCLI-D-14-00488.1

SNOTEL (2022). *Natural Resources Conservation Service National Water and Climate Center—Monthly Snow Data.* https://wcc.sc.egov.usda.gov/nwcc/rgrpt?report=snowmonth&state=UT

Song, S. Y., Yeh, S. W., & Jo, H. S. (2021). Changes in the Characteristics of the North Pacific Jet as a Conduit for US Surface Air Temperature in Boreal Winter across the Late 1990s. *Journal of Climate, 34,* 6841-6853. https://doi.org/10.1175/JCLI-D-20-0353.1

Stahle, D. W. (2020). Anthropogenic Megadrought. *Science, 368,* 238-239. https://doi.org/10.1126/science.abb6902

Sung, M.-K., Kim, B.-M., Baek, E.-H., Lim, Y.-K., & Kim, S.-J. (2016). Arctic-North Pacific Coupled Impacts on the Late Autumn Cold in North America. *Environmental Research Letters, 11,* 084016. https://doi.org/10.1088/1748-9326/11/8/084016

Takahashi, K., Aliaga-Nestares, V., Avalos, G., Bouchon, M., Castro, A., Cruzado, L., & Quispe, N. (2018). The 2017 Coastal El Niño [State of the Climate in 2017]. *Bulletin of American Meteorological Society, 99,* S210-S211.

USDA (2022). *SNOTEL Report Generator 2.0.* https://wcc.sc.egov.usda.gov/reportGenerator

USGS (2022). *National Water Information System.* https://waterdata.usgs.gov/ut/nwis/rt

USGS (2023). *Atmospheric Warming, Loss of Snow Cover, and Declining Colorado River Flow.* https://www.usgs.gov/mission-areas/water-resources/science/atmospheric-warming-loss-snow-cover-and-declining-colorado

Wang, F., Liu, Z., & Notaro, M. (2013). Extracting the Dominant SST Modes Impacting North America's Observed Climate. *Journal of Climate, 26,* 5434-5452. https://doi.org/10.1175/JCLI-D-12-00583.1

Wang, S.-Y., Gillies, R. R., & Reichler, T. (2012). Multidecadal Drought Cycles in the Great Basin Recorded by the Great Salt Lake: Modulation from a Transition-Phase Teleconnection. *Journal of Climate, 25,* 1711-1721. https://doi.org/10.1175/2011JCLI4225.1

Wise, E. K. (2010). Spatiotemporal Variability of the Precipitation Dipole Transition Zone in the Western United States. *Geophysical Research Letters, 37,* Article No. L07706. https://doi.org/10.1029/2009GL042193

WRCC (2021). *Welcome to SC ACIS Version 2.* http://scacis.rcc-acis.org

Yeh, S.-W., Wang, G., Cai, W., & Park, R. J. (2022). Diversity of ENSO-Related Surface Temperature Response in Future Projection in CMIP6 Climate Models: Climate Change Scenario versus ENSO Intensity. *Geophysical Research Letters, 49,* e2021GL096135. https://doi.org/10.1029/2021GL096135

Yu, J.-Y., Zou, Y., Kim, S. T., & Lee, T. (2012). The changing Impact of El Niño on US Winter Temperatures. *Geophysical Research Letters, 39,* Article No. L15702. https://doi.org/10.1029/2012GL052483

Zhang, P., & Wu, Z. (2021). Reexamining the Connection of El Niño and North American Winter Climate. *International Journal of Climatology, 41,* 6133-6144. https://doi.org/10.1002/joc.7204